

Rapidly Rotating Fermions in an Anisotropic Trap

N. Ghazanfari*

Department of Physics, Middle East Technical University, 06531 Ankara, Turkey

M. Ö. Oktel†

Department of Physics, Bilkent University, 06800 Ankara, Turkey

(Dated: March 24, 2021)

We consider a cold gas of non-interacting fermions in a two dimensional harmonic trap with two different trapping frequencies $\omega_x \leq \omega_y$, and discuss the effect of rotation on the density profile. Depending on the rotation frequency Ω and the trap anisotropy ω_y/ω_x , the density profile assumes two qualitatively different shapes. For small anisotropy ($\omega_y/\omega_x \ll \sqrt{1 + 4\Omega^2/\omega_x^2}$), the density consists of elliptical plateaus of constant density, corresponding to Landau levels and is well described by a two dimensional local density approximation. For large anisotropy ($\omega_y/\omega_x \gg \sqrt{1 + 4\Omega^2/\omega_x^2}$), the density profile is Gaussian in the strong confining direction and semicircular with prominent Friedel oscillations in the weak direction. In this regime, a one dimensional local density approximation is well suited to describe the system. The crossover between the two regimes is smooth where the step structure between the Landau level edges turn into Friedel oscillations. Increasing the temperature causes the step structure or the Friedel oscillations to wash out leaving a Boltzmann gas density profile.

I. INTRODUCTION

Rotating ultracold gases have received a lot of attention after the initial experimental demonstration of vortices and vortex lattices in a rotating Bose Einstein condensate[1, 2, 3]. Beyond vortex physics these experiments hold promise to create clean, controllable environments to investigate interesting quantum phases brought upon by the unusually high effective magnetic fields created by rotation. There are both theoretical proposals and experimental efforts to investigate vortex lattice melting[4, 5], Fractional Quantum Hall states [6, 7, 8, 9] and BEC-BCS crossover for rotating gases[10, 11, 12, 13].

The usual procedure for rotating gas experiments start by pumping large amount of angular momentum into the cloud by various rotation methods[2, 3]. Later, confining the gas into trap that is as isotropic as possible to preserve angular momentum, the system settles into a ground state that is rotating at some equilibrium frequency. Another alternative route, which is used in at least one experiment[14], is to create a rotating anisotropic trap with some fixed rotation frequency and wait for the system to reach the ground state at this fixed rotation frequency. This procedure allows for one more control parameter, the trap anisotropy, and is theoretically interesting as it allows the system to smoothly go from a two dimensional regime for small anisotropy to a one dimensional regime for large anisotropy.

The single particle Hamiltonian for a rotating anisotropic trap is exactly diagonalizable, where the eigenenergies can be found by a Bogoliubov transformation[15, 16]. However, a closed form expression for the real space wavefunctions has not been given until recently[17]. The investigations of rotating anisotropic trap systems have focused either on the properties of vortices, or dynamics in the extremely anisotropic limit[18, 19, 20]. All of these studies concern the behavior of interacting Bosons in an anisotropic rotating trap. The interaction strength creates another energy scale which complicates the crossover between the one dimensional and two dimensional regimes of the anisotropic trap.

In this study, we consider the density profile for a gas of non-interacting fermions in a rotating anisotropic trap. Because of the Pauli suppression of s-wave scattering, spin polarized ultracold fermi gases are naturally non-interacting. The absence of another energy scale related to interactions simplifies the physics considerably and reveals how the anisotropic trap smoothly connects the one dimensional regime to two dimensional regime.

The density profile for non-interacting fermions are easily calculated numerically by summing the densities of individual eigenstates. For the rotating anisotropic trap the wavefunctions consist of a exponential part multiplying a Hermite polynomial of a complex coordinate[17]. The recursion relation for Hermite polynomials allows for fast and accurate numerical calculation of the density, enabling us to calculate the exact density for thousands of particles for any rotation frequency or anisotropy.

*Electronic address: gnader@newton.physics.metu.edu.tr

†Electronic address: oktel@fen.bilkent.edu.tr

The numerically calculated density profiles clearly show two distinct regimes. For small anisotropy the density profile consists of a ziggurat like structure of elliptical density plateaus. The density inside a plateau is an integer times $\frac{\gamma}{2\pi}$ where γ is a function of trap frequencies and rotation. Each plateau is clearly identified to belong to a Landau Level, and this regime can be understood as a small deformation of the quantized density profile in an isotropic rotating trap which was first discussed by Ho and Ciobanu[21]. As the trap anisotropy is increased, the plateau structure is replaced by a profile that is Gaussian in the strongly confined direction and a sum of semicircles in the weakly confined direction. Friedel oscillations of the density become prominent as this switching happens, and for very large anisotropy the Landau Level quantization is replaced by quantization of the wavefunction along the transverse, *i.e* strongly confined, direction. The density profiles give a striking example for smooth connection between the two dimensional and one dimensional physics.

The paper is organized as follows: We review the single particle energies and wavefunctions in the next section and give the expressions for the wavefunctions in the lowest five Landau levels. In section III we show that the crossover from two to one dimension is already evident in the energy spectra and define the two regimes quantitatively. Section IV focuses on the numerical density profiles and the description of the properties in both regimes. We also investigate the density profile analytically, and discuss one dimensional and two dimensional local density approximation methods along with Friedel oscillations. Section V contains the numerical results at finite temperature. We conclude in section VI by briefly discussing the experimental consequences of our results and indicating directions for future investigations.

II. SINGLE PARTICLE PROBLEM

We start by considering the single particle physics in a two dimensional rotating anisotropic trap. In this section, we review the results obtained by Fetter, who obtained expressions for the wavefunctions in the Lowest Landau level in reference [17].

Our discussion throughout the paper will be limited to behavior in two dimensions. With this limitation, we are able to focus on the physics of switching between one and two dimensional regimes without the complications introduced by the motion in the third dimension. Our results can be extended to three dimensional systems quite easily if there is strong confinement in the third dimension or if the potential in the third dimension is slowly varying[21]. Both of these limits are routinely realized in ultracold atom experiments.

The Hamiltonian for a single particle in a two dimensional anisotropic harmonic trap can be written in the rotating frame as

$$\mathcal{H} = \frac{1}{2M} (p_x^2 + p_y^2) + \frac{1}{2}M\omega_x^2 x^2 + \frac{1}{2}M\omega_y^2 y^2 - \Omega L_z. \quad (1)$$

Here M is the mass of the particle, the angular momentum in the z direction L_z is given as $L_z = xp_y - yp_x$, and Ω is the rotation frequency. The trapping frequencies along the x and y directions are ω_x, ω_y , respectively. Without loss of generality we take $\omega_y \geq \omega_x$, and refer to the y and x directions as the strongly confined and weakly confined directions throughout the paper. The stability of the trapped system depends on the rotation frequency, which requires the rotation frequency to be smaller than the weak confining frequency $\Omega \leq \omega_x$.

It is clear from the single particle Hamiltonian that the system is essentially described by two dimensionless parameters, the anisotropy

$$\tilde{\omega}_y = \frac{\omega_y}{\omega_x} \geq 1, \quad (2)$$

and the scaled rotation frequency

$$\tilde{\Omega} = \frac{\Omega}{\omega_x} \leq 1. \quad (3)$$

All the relevant quantities can be non-dimensionalized by scaling all the lengths by the oscillator length in the x direction $l_x = \sqrt{\hbar/m\omega_x}$, frequencies by ω_x and energies by $\hbar\omega_x$. In the recent literature on rotating anisotropic traps[16, 20] different sets of non-dimensional parameters have been used to describe the system, unnecessarily complicating the interpretation of the results. We avoid increasing this list of dimensionless quantities by following the notation of Fetter[17] closely. Our numerical calculations are done in dimensionless units, and we will explicitly state our scaling where appropriate.

The eigenenergies for the Hamiltonian Eq.(1) can be obtained by a direct diagonalization, or two successive Bogolubov transformations[15, 16]. The eigenstates are labelled by two integers $n \geq 0$ and $m \geq 0$, and the corresponding energy is

$$E_{n,m} = \hbar \left[\left(n + \frac{1}{2}\right)\omega_- + \left(m + \frac{1}{2}\right)\omega_+ \right], \quad (4)$$

where

$$\omega_{\pm}^2 = \omega_{\perp}^2 + \Omega^2 \mp \sqrt{\frac{1}{4}(\omega_y^2 - \omega_x^2)^2 + 4\omega_{\perp}^2\Omega^2}, \quad (5)$$

with $\omega_{\perp}^2 = \frac{1}{2}(\omega_x^2 + \omega_y^2)$. A schematic plot of the energy levels is given in figure 1, where one can observe that if the rotation is rapid $\Omega \approx \omega_x$, then $\omega_+ \ll \omega_-$ and the levels with the same index n are almost degenerate. Using the analogy between a rotating system and a system under a magnetic field, we identify the levels with the same n index to belong to a Landau level, and call n the Landau level index.

While the system is controlled by the two dimensionless parameters in Eqs. (2), (3), a number of other derived parameters give insight into the dynamics and allow one to express results more concisely. The anisotropy of single particle orbits are controlled by two dimensionless parameters

$$\begin{aligned} \beta_+ &= \frac{\omega_x^2 - \omega_+^2 - \Omega^2}{2\Omega\omega_+}, \\ \beta_- &= \frac{\omega_-^2 - \omega_y^2 + \Omega^2}{2\Omega\omega_+}, \end{aligned} \quad (6)$$

both of which are between 0 and 1. We show in the following sections that a particular combination of these parameters

$$c = \frac{1 - \beta_+\beta_-}{1 + \beta_+\beta_-}, \quad (7)$$

controls the switching between the one and two dimensional regimes. The density of particles in a filled Landau level (see Section IV) is related to the frequency

$$\gamma = \frac{\omega_-^2 - \omega_+^2}{2\Omega}. \quad (8)$$

Finally we define the two 'stretched' complex coordinates which control motion in Landau levels

$$\begin{aligned} \xi_+ &= \sqrt{\frac{2M\gamma\beta_+}{\hbar}} \frac{x + i\beta_-y}{1 + \beta_+\beta_-}, \\ \xi_- &= \sqrt{\frac{2M\gamma\beta_-}{\hbar}} \frac{y + i\beta_+x}{1 + \beta_+\beta_-}. \end{aligned} \quad (9)$$

The ground state of the system has the wavefunction

$$\phi_{00} = \frac{1}{\sqrt{\pi a_x a_y}} \exp\left[-\frac{x^2}{2a_x^2} - \frac{y^2}{2a_y^2}\right] \exp\left\{i\frac{Mxy}{\hbar} \left[\frac{\gamma}{1 + \beta_+\beta_-} - \frac{1}{2}\left(\frac{\omega_+}{\beta_+} + \frac{\omega_-}{\beta_-}\right)\right]\right\}, \quad (10)$$

where a_x and a_y are the widths of the Gaussian envelope

$$a_x^2 = \frac{1 + \beta_+\beta_-}{\beta_+} \frac{\hbar}{M\gamma}, \quad a_y^2 = \frac{1 + \beta_+\beta_-}{\beta_-} \frac{\hbar}{M\gamma}. \quad (11)$$

The wavefunctions in the lowest Landau level (LLL) are found by applying the relevant raising operator to be

$$\phi_{m0}(x, y) = \frac{1}{\sqrt{m!}} \left(\frac{c}{2}\right)^{m/2} H_m\left(\frac{\xi_+}{\sqrt{2c}}\right) \phi_{00}(x, y), \quad (12)$$

where H_m is the m^{th} Hermite polynomial.

Another raising operator allows one to generate the wavefunctions in the higher Landau Levels, for example the states in the first excited Landau level have the wavefunction

$$\phi_{m1}(x, y) = \frac{1}{\sqrt{m!}} \left(\frac{c}{2}\right)^{(m-1)/2} \phi_{00}(x, y) \left[\xi_- \frac{c}{2} H_m\left(\frac{\xi_+}{\sqrt{2c}}\right) - 2im\rho H_{m-1}\left(\frac{\xi_+}{\sqrt{2c}}\right)\right], \quad (13)$$

with $\rho = \sqrt{\beta_-\beta_+}/(1 + \beta_+\beta_-)$. We give the wavefunctions for the six lowest Landau levels in the appendix, and use them in the numerical calculations in section III.

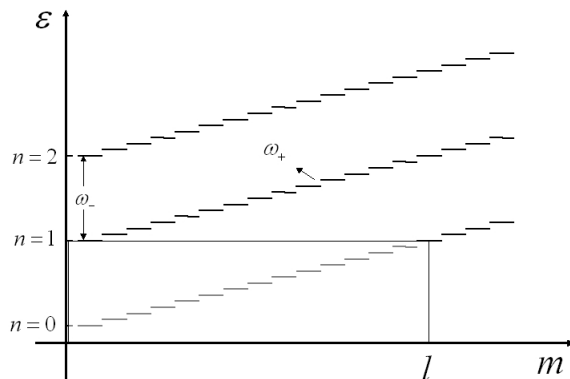


FIG. 1: Energy vs. number of states in each Landau levels. l is the highest number of states within LL's before the next LL is excited.

The wavefunctions given above are remarkable, as they continuously connect the usual 1D harmonic oscillator wavefunctions which have the Hermite polynomial form to 2D Landau level wavefunctions which are (for the lowest Landau level) analytic functions of the complex coordinate $z = x + iy$. In the isotropic limit the m^{th} wavefunction has a m^{th} order zero at the origin. As the anisotropy is turned on the m^{th} order zero immediately breaks up into m first order zeros all of which are on the x axis, as the roots of Hermite polynomials are always real[16]. Increasing anisotropy separates the roots from each other and forces the Gaussian envelope to be more and more anisotropic. In the next section we analyze the one and two dimensional regimes by concentrating on a single quantity that is found from the eigenvalues: the number of energy states in the LLL that have less energy than the first excited Landau Level.

III. ONE AND TWO DIMENSIONAL REGIMES

The switching between the two dimensional and one dimensional regimes is already apparent in the energy spectrum given in Eq.(4). It is instructive to consider two limiting cases. The energies of eigenstates of a rotating isotropic trap given as

$$E_{nm} = \hbar \left[\left(n + \frac{1}{2} \right) (\omega + \Omega) + \left(m + \frac{1}{2} \right) (\omega - \Omega) \right]. \quad (14)$$

The energies for a non-rotating anisotropic trap are

$$E_{n_x n_y} = \hbar \left[\left(n_x + \frac{1}{2} \right) \omega_x + \left(n_y + \frac{1}{2} \right) \omega_y \right]. \quad (15)$$

Both of these expressions have the same structure, as they are labeled by two non-negative integers, and this structure can be graphically represented as in figure 1. The rotating anisotropic trap system interpolates between these two limits, and a good identifier for this interpolation is the number of lowest Landau Level states that have lower energy than any state in the higher Landau levels. We define

$$l = \frac{\omega_-}{\omega_+}, \quad (16)$$

which is graphically shown in figure 1.

The behavior of l as a function of ω_y/ω_x at fixed rotation frequency Ω/ω_x clearly shows the two regimes (See Fig.(2)). At zero anisotropy, l has its isotropic value $(1 + \tilde{\Omega})/(1 - \tilde{\Omega})$. When the anisotropy is introduced, this value

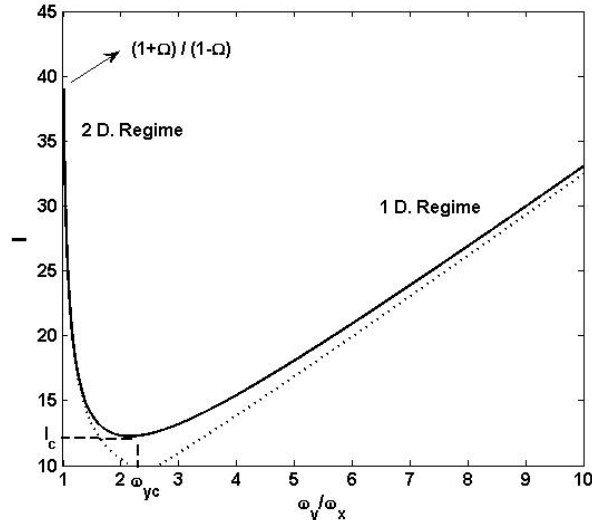


FIG. 2: Solid line shows the behavior of l , number of the stats within two LL's as a function of the anisotropy of the system ω_y/Ω_x . Dashed lines are the asymptotic results for one and two dimensional limits. Here $\omega_{yc} = (1 + 4\Omega/\omega_x)^{1/2}$ is the critical anisotropy where l is minimum. The minimum number of states is given by $l_c = (\frac{8}{1-\Omega/\omega_x})^{1/2}$

quickly decreases as $(\tilde{\omega}_y - 1)^{-1/2}$ and obtains its minimum value of $l_{\min} = \sqrt{8/(1 - \tilde{\Omega})}$ at $\tilde{\omega}_y = \sqrt{1 + 4\tilde{\Omega}^2}$. As the anisotropy is increased further, l increases linearly with $\tilde{\omega}_y$ with slope $1/\sqrt{1 - \tilde{\Omega}^2}$. This linear increase is exactly what is expected in the one dimensional regime as here l would be the ratio of the effective frequencies in the y and x directions,

$$l = \sqrt{\frac{\omega_y^2 - \Omega^2}{\omega_x^2 - \Omega^2}} \simeq \frac{\tilde{\omega}_y}{\sqrt{1 - \tilde{\Omega}^2}}. \quad (17)$$

The degeneracy of the Landau levels in the two regimes originate from two different physical effects. When the anisotropy is small, and the system is in the two dimensional regime, Coriolis force induced by the rotation partially freezes the kinetic energy of the particles and causes the high degeneracy within the Landau levels. For high anisotropy one can think of the energy spectrum in terms of subband quantization in a narrow channel, where each 'Landau Level' actually is formed by states that have the same wavefunction in the tightly confined direction.

The form of the wavefunctions also support this identification based on l . For low anisotropy the wavefunctions peak around an ellipse in the $x - y$ plane, while in the one dimensional regime the density in the x direction shows prominent oscillations, similar to a one dimensional harmonic oscillator wavefunctions. In the next section, we show that the density of a Fermi gas trapped in a rotating anisotropic trap has markedly different behavior in these two regimes.

IV. DENSITY PROFILES

We now consider the density of a gas of N non-interacting spinless fermions in a rotating anisotropic trap. As the real space wavefunctions are known the calculation of density reduces to a sum over the absolute squares of the wavefunctions of all filled eigenstates. Hence the density is given by

$$\rho(x, y) = \sum_{nm} |\phi_{nm}(x, y)|^2 \theta(\mu - E_{nm}), \quad (18)$$

where μ is the chemical potential and the energies E_{nm} and corresponding wavefunctions ϕ_{nm} are given in the previous sections. The chemical potential determined by the number of particles N in the system with the constraint

$$\int dx dy \rho(x, y) = N. \quad (19)$$

The LLL wavefunctions given in sec II are composed of an exponential factor multiplying a Hermite polynomial, and wavunctions in the first few Landau levels given in the appendix also have a similar structure. Hermite polynomials, like other orthogonal polynomial satisfy a recursion relation[22]

$$H_{n+1}(x) = 2xH_n(x) - 2nH_{n-1}(x), \quad (20)$$

which enables rapid and accurate numerical evaluation of the wavefunctions. Because of the recursive structure, the density sum Eq.(18) can also be calculated numerically at very low computational cost. We calculated density profiles for up to $N = 2000$ particles, for parameter values such that all the particles reside in the lowest six Landau Levels.

In figure 3, we display the density profiles for $N = 1000$ particles with fixed rotation frequency $\Omega/\omega_x = 0.999$, for different values of anisotropy. These parameters demonstrate the general behavior of the density profile when the particles are distributed over the first few Landau levels. For small anisotropy the density profile mainly consists of steps, with small regions of switching between them. Each plateau is clearly linked with a Landau level, and defines an elliptical area of almost constant density. As shown below, the density contribution from a filled Landau level is $\rho = \frac{\gamma}{2\pi}$. Thus, the steps have density equal to an integer times $\frac{\gamma}{2\pi}$. For the parameters in Fig.(3a) only the lowest three Landau levels have particles and corresponding steps can be identified clearly. The switching between the n^{th} step and $(n - 1)^{th}$ steps happens with $n - 1$ oscillations in density, which can also be seen in the figure. As the anisotropy is increased the density oscillations between the Landau level steps become more prominent especially in the weak trapping direction. When the anisotropy is within the critical region of switching between two and one dimensional behavior, the steps and the Landau level structure become smeared out. Instead, one can observe the density oscillations becoming prominent throughout the cloud. These oscillations are expected for Fermions, as a sharp Fermi surface cutoff in momentum space results in oscillations in real space, known as Friedel oscillations[23]. For larger values of anisotropy, the density profile assumes a Gaussian shape in the strong confining direction and the familiar semicircular shape of one dimensional trapped fermions in the weak confining direction. Each Landau Level, or rather sub-band in this regime, adds a new semicircle in this direction, thus it is quite easy to observe how many sub-bands are occupied form the density profile (See Fig.(3f)).

In figure 4 we display the density profiles with $N=200$, a low enough particle number so that all the particles remain in the LLL for any value of anisotropy. In this figure, it is easier to discern the character of the change between the two and one dimensional regimes, as one can observe how the flat plateau is replaced by a semicircular shape with Friedel oscillations. Again, the switching happens around the critical value of anisotropy determined from l .

To gain a better understanding of the density profile, we investigate the density sum Eq.(18) in more detail. Let's concentrate on the case for which all the atoms reside in the LLL, for N particles we can write the sum as

$$\begin{aligned} \rho(x, y) &= \sum_{m=0}^N |\phi_{0m}(x, y)|^2 \\ &= \sum_{m=0}^N \frac{1}{m!} \left(\frac{c}{2}\right)^m H_m\left(\frac{\bar{\xi}}{\sqrt{2c}}\right) H_m\left(\frac{\xi}{\sqrt{2c}}\right) \frac{1}{\pi a_x a_y} e^{-x^2/a_x^2 - y^2/a_y^2}. \end{aligned} \quad (21)$$

In the limit $N \rightarrow \infty$ this sum can be evaluated using the generating function for Hermite polynomials. We define

$$S(\bar{z}, z) = \sum_{m=0}^{\infty} \frac{1}{m!} \left(\frac{c}{2}\right)^m H_m(\bar{z}) H_m(z). \quad (22)$$

We use the generating function for Hermite polynomials

$$e^{-t^2 + 2tz} = \sum_m \frac{H_m(z)}{m!} t^m, \quad (23)$$

but regard $t = |t|e^{i\theta}$ as a complex variable. Then the infinite sum can be written as

$$S(\bar{z}, z) = \int_0^{2\pi} \frac{d\theta}{2\pi} \int_0^\infty d|t| 2|t| \exp \left[-\frac{c}{2}(\bar{t}^2 + t^2) + \sqrt{2c}(\bar{t}\bar{z} + tz) - |t|^2 \right]. \quad (24)$$

The resulting Gaussian integral can be evaluated to yield

$$S(\bar{z}, z) = \frac{1}{\sqrt{(1-c)(1+c)}} \exp \left[\frac{1}{2} \frac{c}{1-c} (i(z - \bar{z}))^2 \right] \exp \left[\frac{1}{2} \frac{c}{1+c} (z + \bar{z})^2 \right], \quad (25)$$

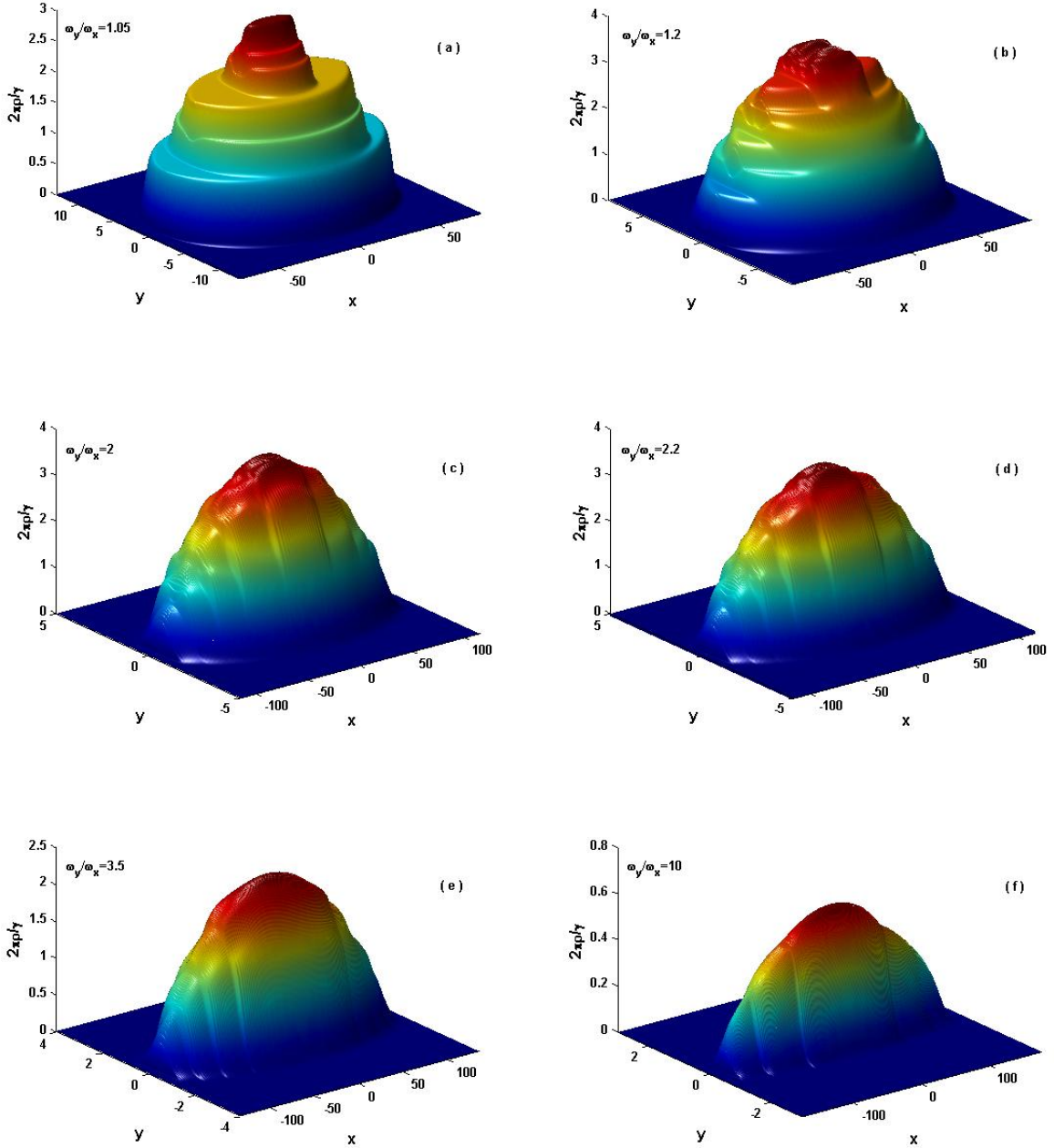


FIG. 3: (color online) Density profiles for fermions at different anisotropy values of the system and fixed number of the particles $N=1000$, and fixed rotation frequency $\Omega/\omega_x = 0.999$. The Friedel oscillations are observed in density profiles of anisotropic cases. The number of LL's that fermions fill at each anisotropy can also be determined by counting the number of plateaus in the density profiles.

which gives the constant density

$$\rho(x, y) = \rho_0 = \frac{1}{\sqrt{1-c^2}} \frac{1}{\pi a_x a_y} = \frac{m\gamma}{2\pi\hbar}. \quad (26)$$

We see that γ is the parameter that controls the density of states per Landau level in an anisotropic trap. In the numerical calculations we see that the steps in the density profile appear at integer multiples of this value. In the two dimensional regime, when the anisotropy is small, the density at the center of the trap quickly reaches this value,

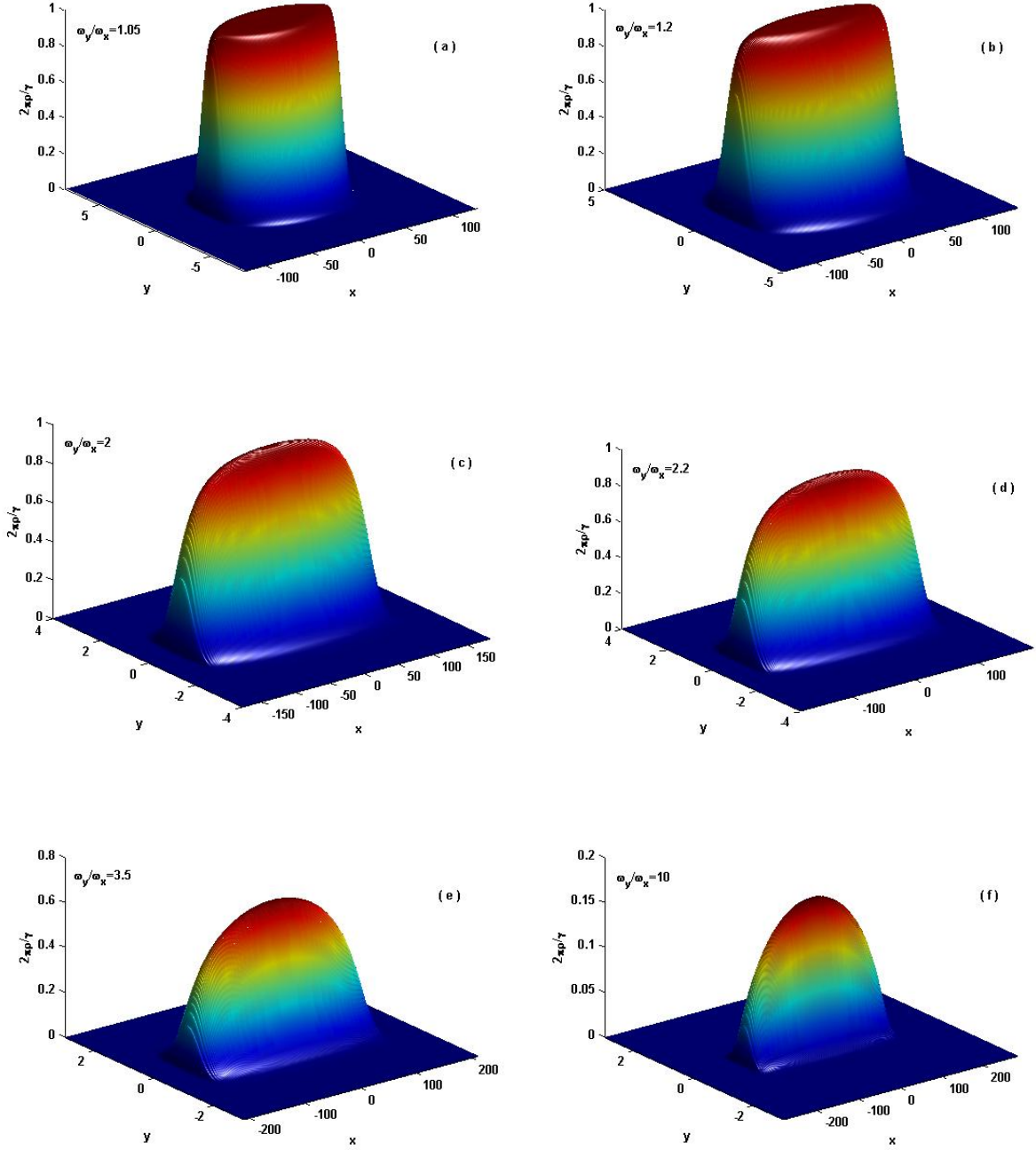


FIG. 4: (color online) Density profiles of fermions at different anisotropy values of the system and fixed number of the particles $N=200$, and fixed rotation parameter $\Omega/\omega_x a = 0.9999$, when all the fermions are settled at the LLL. The Friedel oscillations are also observed for density profiles of anisotropic cases.

even for small number of particles. This is because the contribution of higher wavefunctions to the density near the center is small for low anisotropy.

We must remark that the above result is correct for any anisotropy, i.e. if one puts infinitely many particles into the LLL one would get a constant density. However as the particle number is increased the cloud goes through two very different paths to this constant density profile. In the two dimensional regime, the sum of the density of N particles defines an elliptical region of constant density which grows in size as N is increased. In the one dimensional regime,

density is very anisotropic and shows prominent Friedel oscillations. The frequency of these oscillations decreases as N is increased and the density becomes smooth very slowly with $\sim 1/N$.

The presence of Friedel oscillations in a trapped Fermion system is not unexpected, as the physical reason for their presence is the sharp cutoff at Fermi energy. When one is in the two dimensional Landau Level regime the oscillations are suppressed as locally the maximum allowed density within a Landau level is reached. One can investigate the Friedel oscillations by a simple scaling argument as follows. First let us define the finite sum over Hermite polynomials as

$$S_N(a, b, c) = \sum_{n=0}^N \frac{H_n(\bar{z})H_n(z)}{2^n n!} c^n, \quad (27)$$

with $z = a + ib$. Now because of the infinite sum result we have obtained above we expect two such sums to be related as

$$S_N(a, b, c_2) \cong \sqrt{\frac{1-c_1^2}{1-c_2^2}} S_N\left(\sqrt{\frac{(1+c_1)c_2}{(1+c_2)c_1}} a, \sqrt{\frac{(1-c_1)c_2}{(1-c_2)c_1}} b, c_1\right), \quad (28)$$

if $N \gg 1$ is sufficiently large. Now c_1 can be chosen arbitrarily close to one,

$$\begin{aligned} S_N(a, b, c_1) &= \sum_{n=0}^N \frac{H_n(\bar{z})H_n(z)}{2^n n!} c_1^n \\ &\approx \sum_{n=0}^N \frac{H_n(\bar{z})H_n(z)}{2^n n!} \\ &= S_N(a, b, 1), \end{aligned} \quad (29)$$

provided that $(1-c_1)N \ll 1$. This last sum can be evaluated exactly using Christoffel-Darboux formula[24],

$$\begin{aligned} S_N(a, b, 1) &= \sum_{n=0}^N \frac{H_n(\bar{z})H_n(z)}{2^n n!} \\ &= \frac{H_{N+1}(\bar{z})H_N(z) - H_{N+1}(z)H_N(\bar{z})}{2^{N+1} N! (\bar{z} - z)}. \end{aligned} \quad (30)$$

This exact evaluation and the scaling assumption readily yields a formula for the wavevector of the Friedel oscillations near the center of the trap

$$\rho(x, y=0) = \rho_0 \left(1 + (-1)^N \frac{1}{4N} \cos(k_F x) \right), \quad (31)$$

with

$$k_F l_x = \sqrt{8N/\omega_x} \sqrt{\omega_+ + \omega_- \beta_+ \beta_-}. \quad (32)$$

As expected, this scaling result overestimates the amplitude of the Friedel oscillations, especially in the two dimensional regime. The suppression of oscillations due to limited local density of states is not captured by the scaling assumption. However, scaling correctly describes the wavelength of the oscillations well into the regime where they are too small to observe within our numerical precision.

When the external potential is smooth, a very useful tool to describe the density profile is local density approximation. For the case of a rotating anisotropic lattice we need two different versions of LDA to describe the different behavior in the two regimes.

For the two dimensional regime the effective potential in both strong and weak confining directions are smooth, when compared with the magnetic length imposed by rotation. Thus, it becomes permissible to treat the system locally as a homogenous system with the Landau Level structure. The local density at any point of the gas will be an integer multiple of the density of a filled Landau level $m\Omega/\hbar$. Thus the density profile within the 2D LDA consists of a sequence of elliptical plateaus, which matches well with the numerically calculated density profiles in the 2D regime. Thus 2D LDA is successful in describing the density profile except for the switching regions between the Landau level steps. A typical plot comparing the result of LDA with the calculated density profile is given in Fig.(6).

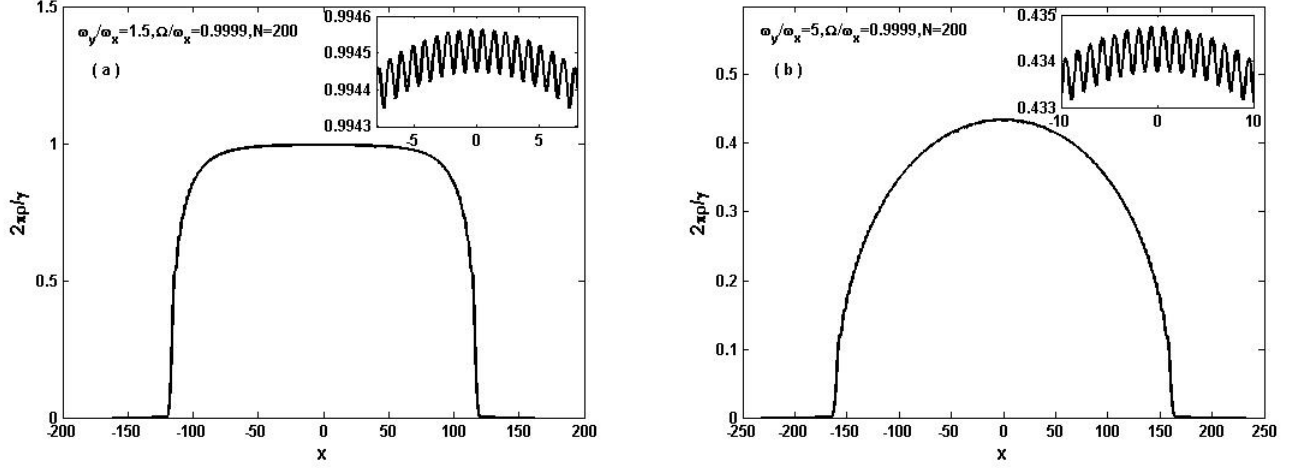


FIG. 5: (a) Density for $N=200$ fermions at $\Omega/\omega_x = 0.9999$, and $\omega_y/\Omega_x = 2.2$. (b) Density for $N=300$ fermions at $\Omega/\omega_x = 0.999$, and $\omega_y/\Omega_x = 2.2$. The insets in both figures highlight the Friedel oscillation in density profiles of the fermions.

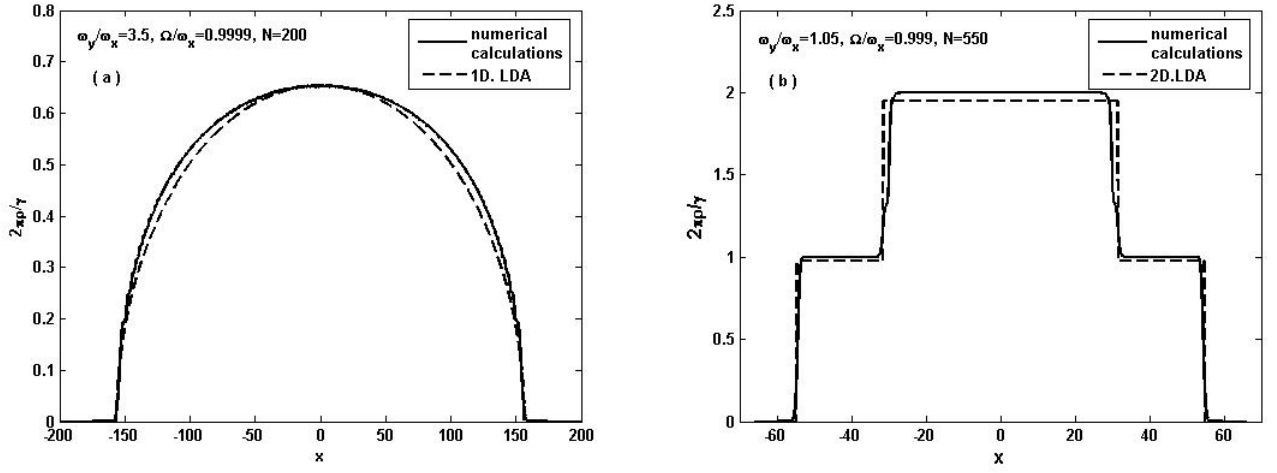


FIG. 6: (a) Density of $N=200$ fermions obtained by direct numerical calculations (solid line), and one dimensional LDA (dashed line) at $\Omega/\omega_x = 0.9999$, and $\omega_y/\Omega_x = 3.5$. (b) Density of $N=325$ fermions obtained by direct numerical calculations (solid line), and two dimensional LDA (dashed line) at $\Omega/\omega_x = 0.99$, and $\omega_y/\Omega_x = 1.2$.

As the anisotropy is increased and the gas enters the crossover regime the step structure in the density profile is no longer observed. This regime is not well described by a two dimensional LDA, as the potential in the strong confining direction is no longer smooth on the scale of magnetic length. However if the anisotropy is increased further, the oscillator length in the strong confining direction becomes much smaller than the magnetic length and another LDA approach becomes feasible. This is exactly the one dimensional regime described in Sec. III.

In the one dimensional regime, the density profile in the strong confining direction is almost the same for all wavefunctions in the same Landau level. Thus we can treat the system within a one dimensional LDA and obtain the usual semicircular profile for the one dimensional fermions

$$\rho(x, y = 0) = \rho(0, 0) \sqrt{1 - \frac{x^2}{L^2}}, \quad (33)$$

where the radius of the cloud is found as

$$L/l_x = \sqrt{\frac{2\mu - \omega_-/\omega_x}{1 - \hat{\Omega}^2}}. \quad (34)$$

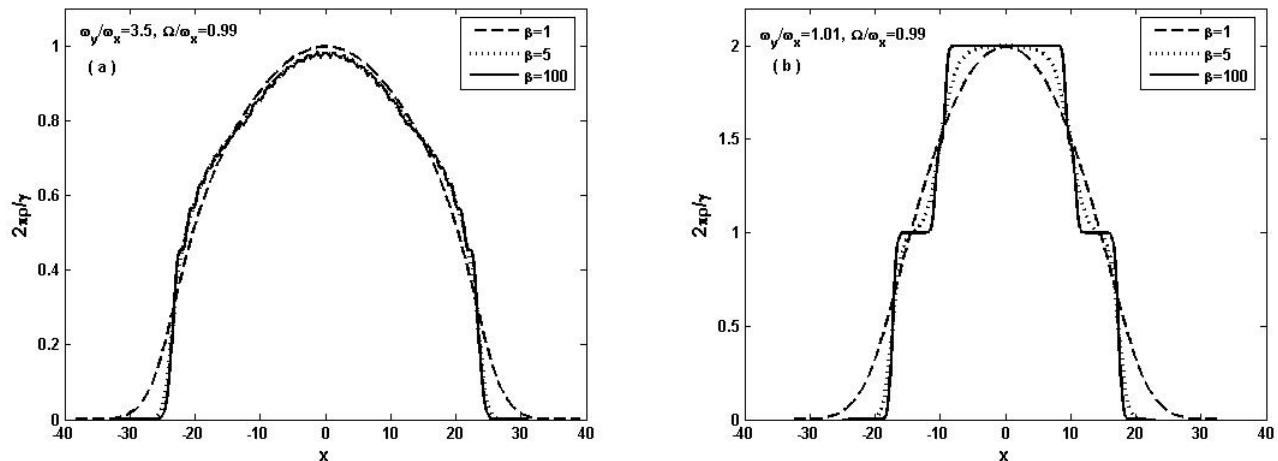


FIG. 7: (a) Density profile for fermions at different temperatures and at $\Omega/\omega_x = 0.99$, and $\omega_y/\Omega_x = 3.5$. (b) Density profile for fermions at different temperatures and at $\Omega/\omega_x = 0.99$, and $\omega_y/\Omega_x = 1.01$. The oscillations (a) and the layered aspect of the profiles (b) are eliminated by temperature. Here $\beta = \frac{\hbar\omega_x}{k_B T}$ is the normalized inverse temperature.

As can be observed in Fig.(6), this approximation describes the density profile in the one dimensional regime reasonably. The agreement increases with increasing anisotropy, but Friedel oscillations can not be captured within the local density approximation. The agreement of one dimensional LDA with the numerically calculated profiles further support our interpretation of the very anisotropic Landau levels as sub-bands formed by quantization in the strong confinement direction.

V. TEMPERATURE EFFECTS

The density profiles given in the previous sections were all calculated at zero temperature. At finite temperature the density profile can be calculated by including the fermi distribution function as

$$\rho(x, y) = \sum_{nm} |\phi_{nm}(x, y)|^2 \frac{1}{\exp \beta(E_{nm} - \mu) + 1}, \quad (35)$$

where $\beta = \frac{1}{k_B T}$ is the inverse temperature.

We calculated density profiles for finite temperatures using the same numerical procedure with the zero temperature case. The temperatures and chemical potentials were chosen to ensure that the occupation of the states higher than the sixth Landau level is less than $\exp[-5] \sim 0.0067$. For the two dimensional regime the step structure of the density profile is expected to be smeared out when the temperature is enough to close the gap between the Landau levels $k_B T \sim \hbar\omega_-$. The calculated density profiles show that the step structure becomes indiscernible below this value, as the transition regions between the Landau level steps dominate the profile. For larger temperatures the profile assumes the gaussian profile as would be expected from a Boltzmann gas.

For the one dimensional regime, the first effect of the finite temperature is to smear out the Friedel oscillations. The relevant energy scale for Friedel oscillations is $\hbar\omega_+$ the separation of energy levels within a Landau level, and as soon as this temperature is reached the density profile becomes smooth, while still obeying the semicircular LDA result. For higher temperatures, once again the density profile becomes Gaussian as would be expected from a Boltzmann gas. The effects of temperature in both regimes is plotted for typical density profiles in figure 7.

VI. CONCLUSION

We show that the density profile of a non-interacting Fermi gas in a rotating anisotropic trap has two distinct regimes depending on the rotation rate and anisotropy. Through numerical calculation and a local density approximation the distinct behavior in the one and two dimensional regimes is observed. For small anisotropy ($\omega_y/\omega_x \ll \sqrt{1 + 4\Omega^2/\omega_x^2}$), the density consists of elliptical plateaus of constant density, corresponding to Landau levels and is well described by

a two dimensional local density approximation. For large anisotropy ($\omega_y/\omega_x \gg \sqrt{1 + 4\Omega^2/\omega_x^2}$), the density profile is Gaussian in the strong confining direction and semicircular with prominent Friedel oscillations in the weak direction. In this regime, a one dimensional local density approximation is well suited to describe the system. The crossover between the two regimes is smooth where the step structure between the Landau level edges turn into Friedel oscillations. Increasing temperature smears out the step structure in the two dimensional regime, and similarly smoothes out the Friedel oscillation in the one dimensional regime.

The exact wavefunctions given for the rotating anisotropic trap provide a smooth one to one mapping between the states in a 2D Landau level and the states in a one dimensional harmonic trap. We expect this mapping to be useful for study of interacting Bose and Fermi systems, going beyond the non-interacting gas in this paper. It would be interesting to see what kind of states are obtained for an extremely elongated trap if this mapping is used on correlated states such as the fractional quantum Hall states in the two dimensional regime. Similarly, certain strongly interacting models in one dimension may accept continuation into two dimension, extending the validity of some exact solutions.

Experiments on rotating ultracold gases have so far focused on isotropic traps, as they mostly rely on the isotropic trap to conserve angular momentum given to the system before equilibrium is established. Nevertheless a rotating anisotropic trap has been demonstrated[1]. A wide array of experiments have displayed the feasibility of designing traps that are strongly confining in one or two dimensions to probe low dimensional physics of quantum gases. All these successes with trap design lead us to conclude that a the trap potential discussed in this paper is within the current experimental capabilities.

A major difficulty in Fermion experiments is creating low enough temperatures to probe quantum mechanical nature of the gas[25, 26, 27, 28, 29, 30]. However as the system considered in this paper is non-interacting, the temperatures needed to observe qualitative features such as density steps is well above the currently obtained lowest temperatures.

The main method employed in measuring density profiles is expansion imaging of the gas, and this method can be used to determine the main features of the density profile such as Landau level step structure or the semicircular density profile in the one dimensional regime. More subtle features, such as Friedel oscillations would require more complicated probes of density such as Bragg spectroscopy[31].

Finally, we remark that the Fermi gas in a rotating anisotropic trap is system that may elucidate the connection between one dimensional physics with dynamics within a Landau level. It would be interesting to extend the study in this paper to interacting fermion systems.

VII. APPENDIX

The ground state wave function of the system is written as

$$\phi_{00} = \frac{1}{\sqrt{\pi a_x a_y}} \exp \left[-\frac{x^2}{2a_x^2} - \frac{y^2}{2a_y^2} \right] \exp \left\{ i \frac{Mxy}{\hbar} \left[\frac{\gamma}{1 + \beta_+ \beta_-} - \frac{1}{2} \left(\frac{\omega_+}{\beta_+} + \frac{\omega_-}{\beta_-} \right) \right] \right\}, \quad (36)$$

and the excited states are obtained by applying the relevant raising operators defined by Fetter[17] on ground state wavefunction. Operator α_+ gives the The excited sates wave functions in each LL, and another one i.e. α_- gives the higher LL states wavefunctions. The wave functions in LLL are obtained to be

$$\varphi_{m0}(x, y) = \frac{1}{\sqrt{m!}} \varphi_{00}(x, y) P_m(\xi_+) \quad (37)$$

where

$$P_m(\xi_+) = \left(\frac{c}{2} \right)^{n/2} H_m \left(\frac{\xi_+}{\sqrt{2c}} \right) \quad (38)$$

The wavefunctions in higher excited Landau levels also are found to be

$$\varphi_{m1}(x, y) = \frac{1}{\sqrt{m!}} \varphi_{00}(x, y) \left[\xi_- P_m(\xi_+) - 2im\rho P_{m-1}(\xi_+) \right], \quad (39)$$

$$\begin{aligned} \varphi_{m2}(x, y) = & \frac{1}{\sqrt{2m!}} \varphi_{00}(x, y) \left\{ \left(\xi_-^2 - c \right) P_m(\xi_+) \right. \\ & - 4im\rho \xi_- P_{m-1}(\xi_+) \\ & \left. - 4m(m-1)\rho^2 P_{m-2}(\xi_+) \right\}, \quad (40) \end{aligned}$$

$$\begin{aligned}
\varphi_{m3}(x, y) = & \frac{1}{\sqrt{3!m!}}\varphi_{00}(x, y) \left\{ \left(\xi_-^3 - 3c\xi_- \right) P_m(\xi_+) \right. \\
& - 6im\rho \left(\xi_-^2 - c \right) P_{m-1}(\xi_+) \\
& - 12m(m-1)\rho^2 \xi_- P_{m-2}(\xi_+) \\
& \left. + 8im(m-1)(m-2)\rho^3 P_{m-3}(\xi_+) \right\}
\end{aligned} \tag{41}$$

$$\begin{aligned}
\varphi_{m4}(x, y) = & \frac{1}{\sqrt{24m!}}\varphi_{00}(x, y) \left\{ \left(\xi_-^4 - 6c\xi_-^2 + 3c^2 \right) P_m(\xi_+) \right. \\
& - 8mi\rho \left(\xi_-^3 - 3c\xi_- \right) P_{m-1}(\xi_+) \\
& - 24m(m-1)\rho^2 \left(\xi_-^2 - c \right) P_{m-2}(\xi_+) \\
& + 32im(m-1)(m-2)\rho^3 \xi_- P_{m-3}(\xi_+) \\
& \left. + 16m(m-1)(m-2)(m-3)\rho^4 P_{m-4}(\xi_+) \right\}
\end{aligned} \tag{42}$$

$$\begin{aligned}
\varphi_{m5}(x, y) = & \frac{1}{\sqrt{120m!}}\varphi_{00}(x, y) \left\{ \left(\xi_-^5 - 10c\xi_-^3 + 15c^2\xi_- \right) P_m(\xi_+) \right. \\
& - 10im\rho \left(\xi_-^4 - 6c\xi_-^2 + 3c^2 \right) P_{m-1}(\xi_+) \\
& - 40m(m-1)\rho^2 \left(\xi_-^3 - 3c\xi_- \right) P_{m-2}(\xi_+) \\
& + 80im(m-1)(m-2)\rho^3 \left(\xi_-^2 - c \right) P_{m-3}(\xi_+) \\
& + 80m(m-1)(m-2)(m-3)\rho^4 \xi_- P_{m-4}(\xi_+) \\
& \left. - 32im(m-1)(m-2)(m-3)(m-4)\rho^5 P_{m-5}(\xi_+) \right\}
\end{aligned} \tag{43}$$

We suggest a general form for the wavefunctions of the excited states:

$$\begin{aligned}
\varphi_{mn}(x, y) = & \frac{1}{\sqrt{n!m!}}\varphi_{00}(x, y) \\
& \times \sum_{k=0}^n \left[(-i)^{n-k} \frac{2^{n-k}}{(n-k)!} \rho^{n-k} \right. \\
& \left. \times \frac{d^{n-k}}{d^{n-k}\xi_-} P_n(\xi_-) \frac{d^{n-k}}{d^{n-k}\xi_+} P_m(\xi_+) \right]
\end{aligned} \tag{44}$$

Acknowledgments

N.G. is supported by TÜBİTAK. M. Ö. O. is supported by TÜBİTAK-KARİYER Grant No. 104T165.

-
- [1] K. W. Madison, F. Chevy, W. Wohlleben, J. Dalibard, Phys. Rev. Lett. **84**, 806, (2000).
 - [2] J. R. Abo-Shaer, C. Raman, J. M. Vogels, and W. Ketterle, Science **292**, 476 (2001).
 - [3] P. C. Haljan, I. Coddington, P. Engels, E. A. Cornell, Phys. Rev. Lett. **87**, 210403 (2001).
 - [4] N.R. Cooper, N.K. Wilkin, and J.M.F. Gunn, Phys. Rev. Lett. **87**, 120405 (2001).
 - [5] J. Sinova, C.B. Hanna, and A.H. MacDonald, Phys. Rev. Lett. **89**, 030403 (2002).
 - [6] M. A. Baranov, K. Osterloh, and M. Lewenstein, Phys. Rev. Lett. **94**, 070404 (2005).
 - [7] A. S. Sorensen, E. Demler, and M. D. Lukin, Phys. Rev. Lett. **94**, 086803 (2005).
 - [8] M. Hafezi, A. S. Sorensen, E. Demler, and M. D. Lukin, Phys. Rev. A **76**, 023613 (2007).

- [9] K. Osterloh, N. Barberan, and M. Lewenstein, *Phys. Rev. Lett.* **99**, 160403 (2007).
- [10] M. Geriner, C. Regal, D. Jin, *Nature* **426**, 537 (2003).
- [11] M. W. Zwierlein, C. A. Stan, C. H. Schunck, S. M. F. Raupach, A. J. Kerman, W. Ketterle, *Phys. Rev. Lett.* **92**, 120403 (2004).
- [12] M. W. Zwierlein, J. Abo-Shaeer, A. Shirotzek, C. H. Schunck, W. Ketterle, *Nature* **435**, 1047 (2005).
- [13] I. Bloch, J. Dalibard, W. Zwerger, *Rev. Mod. Phys.* **80**, 885 (2008).
- [14] P. Rosenbusch, D. S. Petrov, S. Sinha, F. Chevy, V. Bretin, Y. Castin, G. Shlyapnikov, and J. Dalibard, *Phys. Rev. Lett.* **88**, 250403 (2002).
- [15] M. Linn, M. Niemeier, A. L. Fetter, *Phys. Rev. A* **64**, 023602 (2001).
- [16] M. Ö. Oktel, *Phys. Rev. A* **69**, 023618 (2004).
- [17] A. L. Fetter, *Phys. Rev. A* **75**, 013620 (2007).
- [18] S. Sinha, G. V. Shlyapnikov, *Phys. Rev. Lett.* **94**, 150401 (2005).
- [19] P. Sanchez-Lotero, J.J. Palacios, *Phys. Rev. A* **72**, 043613 (2005).
- [20] A. Aftalion, X. Blanc, N. Lerner, *Phys. Rev. A* **79**, 011603(R) (2009).
- [21] T. L. Ho, C. V. Ciobanu, *Phys. Rev. Lett.* **85**, 4648 - 4651 (2000).
- [22] G. B. Arfken, H. J. Weber, *Mathematical Methods for Physicists* (Elsevier Academic Press, 2005).
- [23] J. Friedel, *Nuovo Cimento (Suppl.)* **7**, **287** (1958).
- [24] M. Abramowitz and I. Stegun, *Handbook of Mathematical Functions*, (Dover, New York, 1970).
- [25] B. DeMarco, and D. S. Jin, *Science* **285**, 1703 (1999).
- [26] A. G. Truscott, K. E. Strecker, W. I. McAlexander, G. B. Partridge, and R. G. Hulet, *Science* **291**, 2570 (2001).
- [27] F. Schreck, L. Khaykovich, K. L. Corwin, G. Ferrari, T. Bourdel, J. Cubizolles, and C. Salomon, *Phys. Rev. Lett.* **87**, 080403 (2001).
- [28] S. R. Granade, M.E. Gehm, K. M. OHara, and J. E. Thomas, *Phys. Rev. Lett.* **88**, 120405 (2002).
- [29] Z. Hadzibabic, C. A. Stan, K. Dieckmann, S. Gupta, M.W. Zwierlein, A. Gorlitz, and W. Ketterle, *Phys. Rev. Lett.* **88**, 160401 (2002).
- [30] G. Roati, F. Riboli, G. Modugno, and M. Inguscio, *Phys. Rev. Lett.* **89**, 150403 (2002).
- [31] J. Stenger, S. Inouye, A. P. Chikkatur, D. M. Stamper-Kurn, D. E. Pritchard, and W. Ketterle, *Phys. Rev. Lett.* **82**, 4569-4573 (1999).